



AFRL-AFOSR-JP-TR-2018-0067

---

Integrated Multifunctional Stretchable Nanofibers for Novel  
Energy Applications

Alex K Y Jen  
UNIVERSITY OF WASHINGTON  
4333 BROOKLYN AVE NE  
SEATTLE, WA 98195-0001

---

09/19/2018  
Final Report

DISTRIBUTION A: Distribution approved for public release.

Air Force Research Laboratory  
Air Force Office of Scientific Research  
Asian Office of Aerospace Research and Development  
Unit 45002, APO AP 96338-5002

<b>REPORT DOCUMENTATION PAGE</b>				<i>Form Approved</i> OMB No. 0704-0188	
<p>The public reporting burden for this collection of information is estimated to average 1 hour per response, including the time for reviewing instructions, searching existing data sources, gathering and maintaining the data needed, and completing and reviewing the collection of information. Send comments regarding this burden estimate or any other aspect of this collection of information, including suggestions for reducing the burden, to Department of Defense, Executive Services, Directorate (0704-0188). Respondents should be aware that notwithstanding any other provision of law, no person shall be subject to any penalty for failing to comply with a collection of information if it does not display a currently valid OMB control number.</p> <p><b>PLEASE DO NOT RETURN YOUR FORM TO THE ABOVE ORGANIZATION.</b></p>					
<b>1. REPORT DATE (DD-MM-YYYY)</b> 20-09-2018		<b>2. REPORT TYPE</b> Final		<b>3. DATES COVERED (From - To)</b> 28 May 2015 to 27 May 2018	
<b>4. TITLE AND SUBTITLE</b> Integrated Multifunctional Stretchable Nanofibers for Novel Energy Applications				<b>5a. CONTRACT NUMBER</b>	
				<b>5b. GRANT NUMBER</b> FA2386-15-1-4106	
				<b>5c. PROGRAM ELEMENT NUMBER</b> 61102F	
<b>6. AUTHOR(S)</b> Alex K Y Jen				<b>5d. PROJECT NUMBER</b>	
				<b>5e. TASK NUMBER</b>	
				<b>5f. WORK UNIT NUMBER</b>	
<b>7. PERFORMING ORGANIZATION NAME(S) AND ADDRESS(ES)</b> UNIVERSITY OF WASHINGTON 4333 BROOKLYN AVE NE SEATTLE, WA 98195-0001 US				<b>8. PERFORMING ORGANIZATION REPORT NUMBER</b>	
<b>9. SPONSORING/MONITORING AGENCY NAME(S) AND ADDRESS(ES)</b> AOARD UNIT 45002 APO AP 96338-5002				<b>10. SPONSOR/MONITOR'S ACRONYM(S)</b> AFRL/AFOSR IOA	
				<b>11. SPONSOR/MONITOR'S REPORT NUMBER(S)</b> AFRL-AFOSR-JP-TR-2018-0067	
<b>12. DISTRIBUTION/AVAILABILITY STATEMENT</b> A DISTRIBUTION UNLIMITED: PB Public Release					
<b>13. SUPPLEMENTARY NOTES</b>					
<b>14. ABSTRACT</b> Fiber-based electronics is an emerging research field and attracting considerable attention in materials, medical, and engineering communities due to their great potential of being woven into smart electronic textiles for future wearable devices and combat-related missions of soldiers. In the Taiwanese Nanoscience Program, the Jen group is responsible for developing proper charge-transporting layers (CTLs) for the fiber-based target electronics, providing expertise in interfacial engineering, and applying them to polymer and hybrid perovskite solar cells. In this program, we have developed novel low temperature solution processable CTLs and interface materials to facilitate the fabrication of high-performance and stable perovskite solar cells (PVSCs). Now, efforts have been extended to develop crosslinkable CTLs and non-fullerene acceptors for wide bandgap polymers, and to develop passivation methods based on graded fullerene heterojunction in low bandgap Pb-Sn binary PVSCs for fiber-based electronic applications.					
<b>15. SUBJECT TERMS</b> Fibers, Composites, Energy Conversion, Flexible Devices, Electro-Spinning, Stretchable Electronic Textile, Stretchable Fiber Electrodes					
<b>16. SECURITY CLASSIFICATION OF:</b>			<b>17. LIMITATION OF ABSTRACT</b>	<b>18. NUMBER OF PAGES</b>	<b>19a. NAME OF RESPONSIBLE PERSON</b>
<b>a. REPORT</b>	<b>b. ABSTRACT</b>	<b>c. THIS PAGE</b>			WINDER, SHEENA
Unclassified	Unclassified	Unclassified	SAR		<b>19b. TELEPHONE NUMBER (include area code)</b> +81-42-511-2008

## Final Report for AOARD (FA2386–15–1–4106)

### “Integrated Multifunctional Stretchable Nanofibers for Novel Energy Applications”

June 12, 2018

Alex K.-Y. Jen, [ajen@uw.edu](mailto:ajen@uw.edu),  
University of Washington, Materials Science and Engineering  
University of Washington, Seattle, WA 98195-2120

Period of Performance: 9/28/2015 – 5/27/2018

**Abstract:** Fiber-based electronics is an emerging research field and attracting considerable attention in materials, medical, and engineering communities due to their great potential of being woven into smart electronic textiles for future wearable devices and combat-related missions of soldiers. However, the device performance of fiber-based electronic devices is still lagging behind the planar counterparts due to the lack of proper interfacial materials and electrodes. In the Taiwanese Nanoscience Program, the Jen group is responsible for developing proper charge-transporting layers (CTLs) for the fiber-based target electronics, providing expertise in interfacial engineering, and applying them to polymer and hybrid perovskite solar cells. In this program, we have developed novel low-temperature solution processable CTLs and interface materials to facilitate the fabrication of high-performance and stable perovskite solar cells (PVSCs). Now, we have extended our efforts to develop crosslinkable CTLs and non-fullerene acceptors for wide bandgap polymers, and to develop passivation methods based on graded fullerene heterojunction in low bandgap Pb-Sn binary PVSCs for fiber-based electronic applications.

#### Introduction:

In the past few years, stretchable electronics have attracted extensive research interests in diverse communities because of their promising merits to cover complex (non-flat) surfaces with functions adaptable with human movements.<sup>[1-3]</sup> Due to the challenges of applying brittle inorganic semiconductors onto these stretchable electronics, flexible organic semiconductors become the most promising material system for wearable electronics, especially for organic semiconductors forming fibers. Compared to a thin film, the fiber network structure can release shear stress more easily and tolerate much higher stretch strains without deteriorating the properties of employed semiconductors.<sup>[4-7]</sup> Moreover, multifunctional electronic applications can be accomplished by incorporating combination of semiconducting/conducting components into the organic fibers, some even as nanofibers. Eventually, such multifunctional organic fibers can be woven with textile fiber fabrics into “Smart Clothes” for both civilian and soldiers for desired functions.

To fulfill semiconducting organic fibers into practical applications, several challenges need to be addressed. First, the typically used metal wire core electrodes need to be replaced since its

rigidity and heavy weights restrain the wearable textile applications. Second, the performance of the fiber devices needs to be significantly improved in order to compete with thin-film counterparts. The lower performance of the fiber-based electronics will significantly hinder the deployment of these devices for practical applications. Finally, significant efforts need to be made to integrate different functionalities into single electronic fibers and weave them into applicable smart clothes.

To enhance the performance of the fiber-based electronics, interfacial engineering is an important area, not only to reduce the interfacial barrier to maximize the device performance but also to improve the wettability and increase the adhesion between the constituent interlayers.<sup>[8]</sup> The functions of the interfacial materials can be summarized into four main parts: (1) Tuning the energy alignment at the electrode/active layer interface; (2) Facilitating the charge extraction efficiency in device and improving the charge selectivity of electrodes; (3) Controlling the surface properties of interfaces to modulate the morphology of the active layer grown above; (4) Improving interfacial stability and adhesion between the active layer and electrodes.<sup>[9]</sup> By providing expertise of Jen group in interface engineering, including the development of electron- and hole-extraction materials and functionalized self-assembled monolayers (SAMs) developed for polymer and hybrid perovskite solar cells, we have aimed to integrate our materials and interface engineering knowhow into the fiber-shaped devices development.

In this program, we have developed low-temperature solution processable advanced charge-transporting interlayers (CTLs) to facilitate the fabrication of stable high-performance perovskite solar cells (PVSCs). As previously reported, we have developed a new class of electron-transporting layers (ETLs) that can replace TiO<sub>2</sub> realizing efficient conventional n-i-p PVSCs. Now, we have extended our efforts to develop crosslinked CTLs, mapping non-fullerene acceptors for wide bandgap polymers for polymer solar cells, and to develop passivation methods based on graded fullerene heterojunction in low bandgap Pb-Sn binary PVSCs for fiber-based electronic applications. Our recent research progresses in these area are summarized in this report.

## **Results and Discussion:**

### ***Development of crosslinked charge-transporting layers for highly efficient and stable perovskite solar cells***

Although the performance of PVSCs has already been demonstrated to rival those of the prevailing inorganic counterparts, the device's long-term stability under thermal, photo-, and moisture stresses has been raised as one major challenge before the commercialization of this technology. To provide possible solutions to overcome this hurdle, we have designed and synthesized a crosslinkable n-type conjugated molecule, c-HATNA, that can be crosslinked at a relatively low temperature (~110 °C) to form a robust ETL on top of the perovskite layer.

The crosslinked c-HATNA film is hydrophobic and possesses very good thermal stability, enabling the fabrication of stable inverted PVSCs (ITO/NiO/CH<sub>3</sub>NH<sub>3</sub>PbI<sub>3</sub>/c-HATNA/bis-C60/Ag). By proper doping to increase its electron-transporting property, a high PCE of 18.21% was obtained with respectable moisture and thermal stability without encapsulation. Moreover, this c-HATNA ETL can be used in conjunction with another crosslinkable hole-transporting layer (HTL) c-TCTA-BVP to fabricate an all-crosslinked CTLs (substrate/c-TCTA-BVP/ CH<sub>3</sub>NH<sub>3</sub>PbI<sub>3</sub>/c-HATNA/bis-C60 /Ag) for PVSC. Benefitting from the low-temperature crosslinking reactions, the derived cells can achieve high PCE of 16.08% and 13.42% on rigid and flexible substrates, respectively. More importantly, the device with all-crosslinked CTLs showed impressive thermal stability in ambient without encapsulation, retaining almost 70% of its initial PCE after being heated at 70 °C for 300 h.

**Figure 1a** shows a crosslinkable HATNA derivative, 3,9,14-trifluorodiquinoxalino [2,3-a:2',3'-c] phenazine -2,8, 15-trisulfinyl) tris(propene-3,1-diyl) tris(2-methylacrylate) (namely c-HATNA). This compound comprises a HATNA core with three crosslinkable side-chains, in which the acrylate group can be crosslinked easily in solid state. In order to efficiently crosslink c-HATNA, its thermal transition properties with and without the assistance of PETMP were investigated first by differential scanning calorimetry (DSC). As

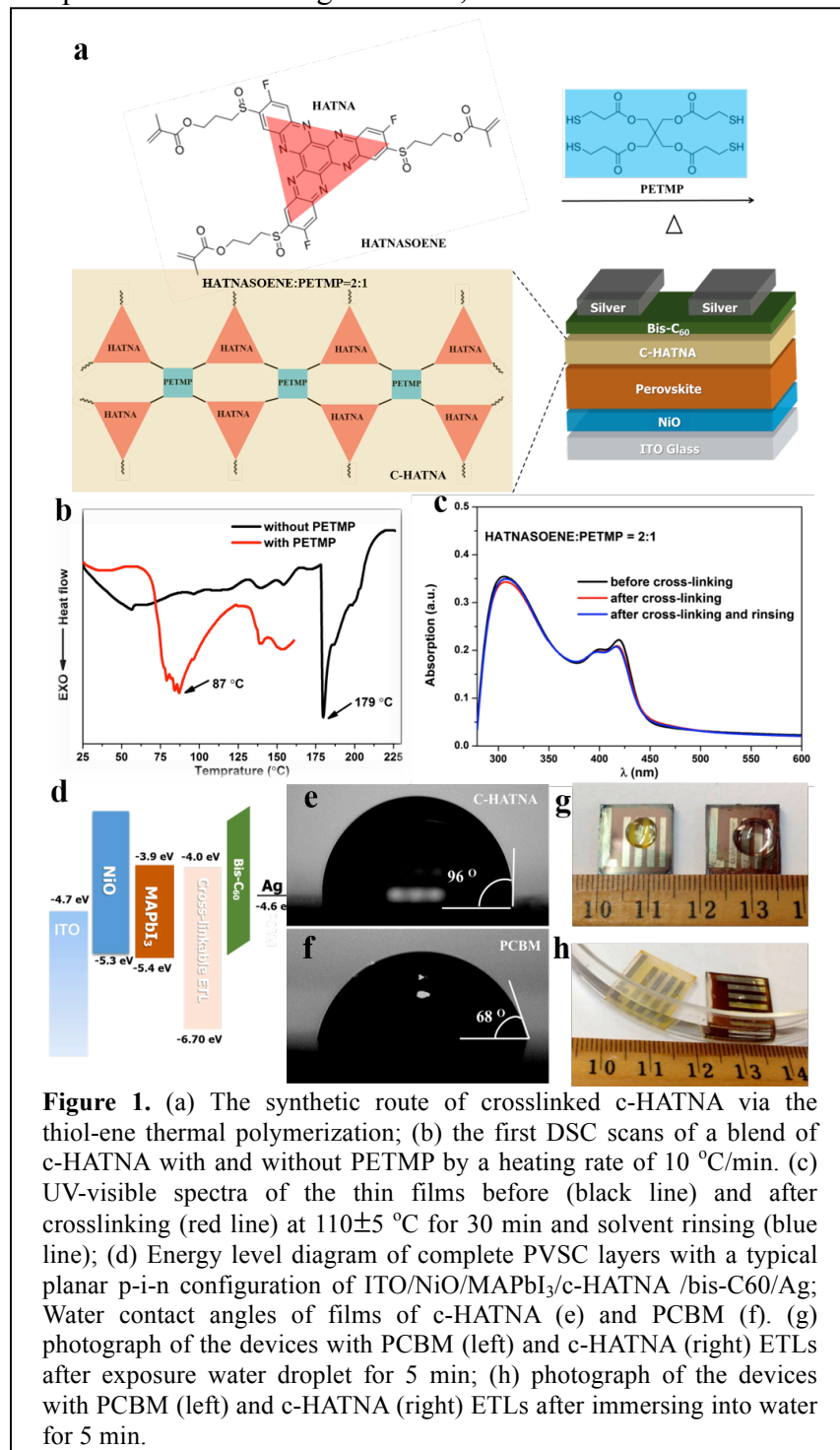


**Figure 1.** (a) The synthetic route of crosslinked c-HATNA via the thiol-ene thermal polymerization; (b) the first DSC scans of a blend of c-HATNA with and without PETMP by a heating rate of 10 °C/min. (c) UV-visible spectra of the thin films before (black line) and after crosslinking (red line) at 110±5 °C for 30 min and solvent rinsing (blue line); (d) Energy level diagram of complete PVSC layers with a typical planar p-i-n configuration of ITO/NiO/MAPbI<sub>3</sub>/c-HATNA /bis-C60/Ag; Water contact angles of films of c-HATNA (e) and PCBM (f). (g) photograph of the devices with PCBM (left) and c-HATNA (right) ETLs after exposure water droplet for 5 min; (h) photograph of the devices with PCBM (left) and c-HATNA (right) ETLs after immersing into water for 5 min.

shown in **Figure 1b**, the crosslinking temperature estimated from the broad exothermic peak decreased significantly from  $\sim 179$  °C for the pristine c-HATNA film to  $\sim 87$  °C for the c-HATNA/PETMP blend film. This result clearly indicates the fast and complete thermal crosslinking of c-HATNA/PETMP film proceeds at a much lower temperature due to rapid thiol-ene reaction. This provides more tolerance for the perovskite layer below compared to most of the traditional thermal crosslinking reactions reported so far. Presented in **Figure 1c** is the UV-vis absorption spectra of the c-HATNA/PETMP blend film (on glass substrate) before and after crosslinking at 110 °C, wherein the crosslinked film was further rinsed by various organic solvents (acetone, dichloromethane (DCM), toluene, and tetrahydrofuran (THF)) after crosslinking to remove any un-crosslinked residues. A high optical quality film obtained after solvent rinsing with similar absorption intensity (compared to the as cast film with similar thickness before rinsing), indicating good solvent resistance as a result of crosslinking.

As shown in **Figure 1c**, the absorption edge of the c-HATNA film is located at  $\sim 460$  nm, corresponding to an optical bandgap of 2.70 eV. The onset of the first oxidative potential versus Fc/Fc<sup>+</sup> was found to be -1.12 eV, corresponding to the highest occupied molecular orbital (HOMO) level of -6.70 eV which will provide better hole-blocking capability and charge selectivity (**Figure 1d**). Meanwhile, its lowest unoccupied molecular orbital (LUMO) level was estimated to be -4.00 eV, which matches reasonably well with the conduction band minimum (CBM) of CH<sub>3</sub>NH<sub>3</sub>PbI<sub>3</sub> affirming the feasibility of achieving efficient electron transfer between them.

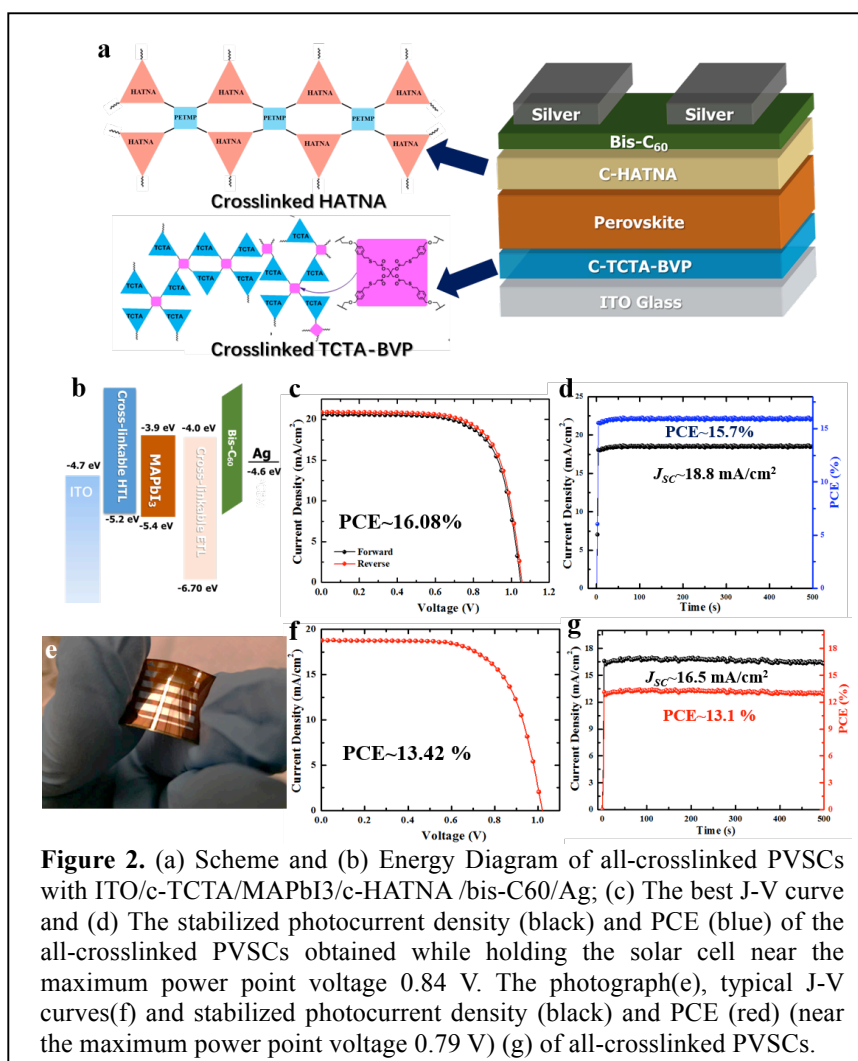
The contact angle measurement (by water droplet) of c-HATNA film was displayed in **Figure 1e**, wherein the c-HATNA and crosslinked film showed a higher contact angle of  $\sim 96^\circ$  and  $\sim 97^\circ$  compared to that ( $\sim 68^\circ$ ) of PCBM (**Figure 1f**). This enhanced hydrophobicity is in part attributed to the introduced alkyl thiol co-crosslinking group which will benefit the moisture stability of the derived inverted PVSC. To realize the waterproof efficacy introduced by c-HATNA, moisture resistance of its derived PVSC were placed under extreme conditions to examine for certain fixed time. First, water was directly dropped on the fabricated device for 5 min as shown in **Figure 1g**. The reference device with a PCBM ETL degraded completely (brown color CH<sub>3</sub>NH<sub>3</sub>PbI<sub>3</sub> changed to yellow color PbI<sub>2</sub>) in 5 s after contacting the water droplets while the sandwiched perovskite film in c-HATNA-derived device remained intact. To better illustrate this, **Figure 1h** showed the photos of the devices immersed in water for 5 min. The PCBM-derived device degraded completely while the c-HATNA-derived device showed impressive waterproof property.

Given these promising results enabled by the c-HATNA ETL, we have further developed a PVSC using all-crosslinked CTLs by replacing the NiO HTL with our previously explored crosslinkable HTL, c-TCTA-BVP. A device with the configuration of ITO/c-TCTA-BVP/CH<sub>3</sub>NH<sub>3</sub>PbI<sub>3</sub>/3 wt% Et<sub>3</sub>N-doped c-HATNA/bis-C60/Ag was fabricated as shown in **Figure 2a** and its corresponding energy level diagram was illustrated in **Figure 2b**, where the CBM and valence band maximum (VBM) of the perovskite layer are aligned with the LUMO and HOMO of the crosslinked ETL and HTL, respectively. Its J-V characteristics measured under AM 1.5 G illumination and a scan rate of 0.1 V s<sup>-1</sup> was present in **Figure 2c**.

As shown, the device derived from the both crosslinked CTLs shows a PCE<sub>MAX</sub> of 16.08%, with a VOC of 1.05 V, a JSC of 20.90 mA cm<sup>-2</sup>, and a FF of 73.3% (under reverse scan). We

noted that the hysteresis appears slightly while the scan rate is gradually increased from  $0.01 \text{ V s}^{-1}$  to  $0.5 \text{ V s}^{-1}$ , which might stem from the interfacial charge traps at the HTL/perovskite interface. The stabilized photocurrent of the top-performing device measured at a constant bias of  $0.84 \text{ V}$  near the MPP was plotted in **Figure 2d**, wherein a steady photocurrent of  $18.8 \text{ mA cm}^{-2}$ , corresponding to a steady PCE of  $15.7\%$ , is achieved, consistent with the performance obtained from J-V measurement. All these results confirm the good reliability of the fabricated devices using the all-crosslinked CTLs.

Since the crosslinking method adopted here can be processed under mild temperatures, we have also fabricated device on a flexible ITO-coated polyethylene naphthalate (PEN) substrate as illustrated in **Figure 2e**. The resultant J-V curve is presented in **Figure 2f** showing a PCE<sub>MAX</sub> of  $13.42\%$ , with a reasonable VOC of  $1.01 \text{ V}$ , a JSC of  $18.82 \text{ mA cm}^{-2}$ , and a FF of  $70.6\%$  (under reverse scan). The lower JSC and FF of the flexible device relative to the rigid counterpart could arise from the higher sheet resistance of ITO/PEN substrate. **Figure 2g** portrays its stabilized photocurrent measured at a constant bias of  $0.79 \text{ V}$  near the MPP, wherein a steady PCE ( $\sim 13.1\%$ ) close to the value obtained from J-V measurement is confirmed.



### *Development of non-fullerene acceptors for wide bandgap polymers for high performance polymer solar cells*

Recently, non-fullerene polymer solar cells (NF-PSCs) with p-type conjugated polymer as donor and n-type non-fullerene small molecule as acceptor have attracted great attentions and made significant progresses.<sup>[10-13]</sup> The PCE of the state-of-the-art NF-PSCs has reached  $13\%$  due to the development of new polymer donors and non-fullerene acceptors.<sup>[14-17]</sup> Among the

non-fullerene acceptors, 2-(3-oxo-2,3-dihydro-1H-inden-1-ylidene)malononitrile and indacenodithiophene (IDT) or indacenodithieno[3,2-b]thiophene (IDTT)-combined small molecules (ITIC and its analogues) are demonstrated as the most successful candidates for NF-PSCs, because of their impressive advantages of easy accessibility, strong absorption in the visible region, easily tunable energy levels, and superior morphological stability in the blend film.<sup>[10-14]</sup>

To match with those novel acceptors and achieve better device performance, considerable efforts have been dedicated to the development of D-A type wide bandgap (WBG) polymer donors (optical bandgap > 1.8 eV) and proved to be an effective strategy.<sup>[18-21]</sup> However, it is a daunting challenge to develop efficient WBG polymer donors to match with NIR acceptors, not to mention for ITIC-analogues and NIR acceptors simultaneously because the suitable energy levels between donor and acceptor is another prerequisite for achieving a high PCE in addition to a broad complementary absorption spectrum.

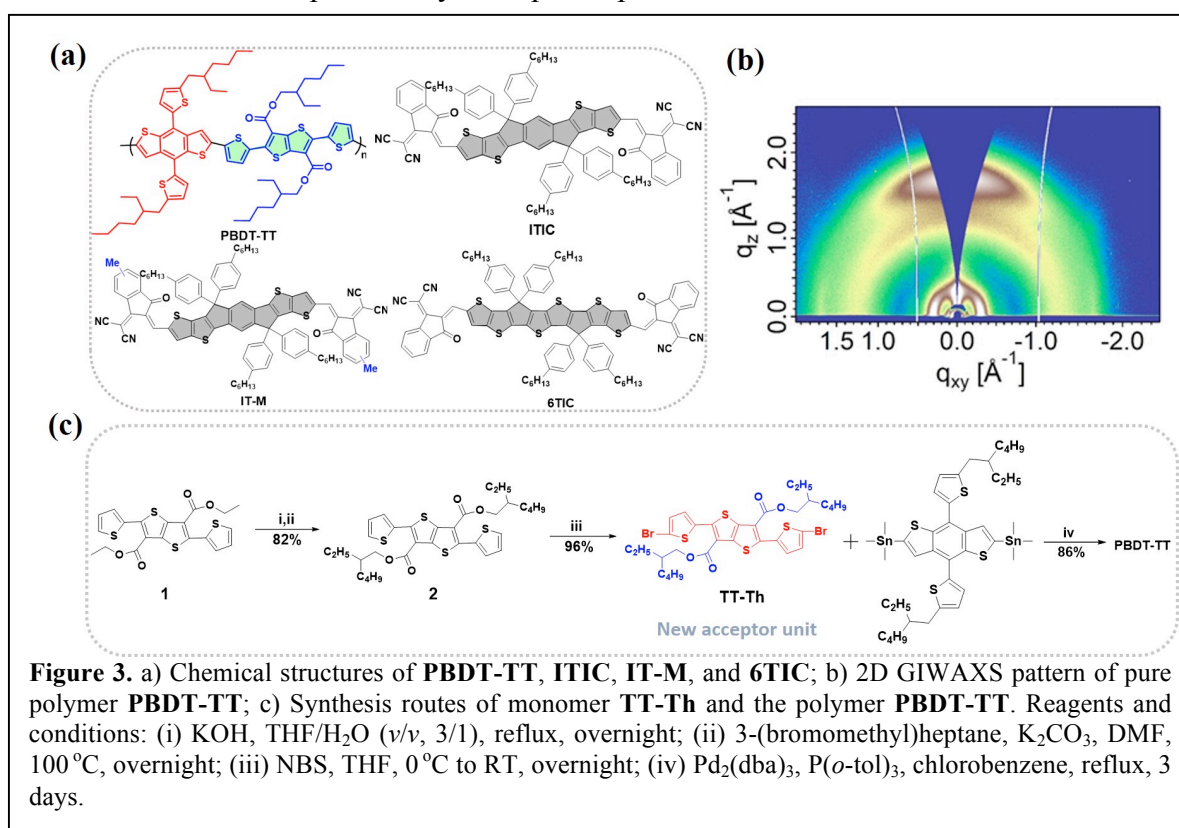


**Figure 3.** a) Chemical structures of PBDT-TT, ITIC, IT-M, and 6TIC; b) 2D GIWAXS pattern of pure polymer PBDT-TT; c) Synthesis routes of monomer TT-Th and the polymer PBDT-TT. Reagents and conditions: (i) KOH, THF/H<sub>2</sub>O (v/v, 3/1), reflux, overnight; (ii) 3-(bromomethyl)heptane, K<sub>2</sub>CO<sub>3</sub>, DMF, 100 °C, overnight; (iii) NBS, THF, 0 °C to RT, overnight; (iv) Pd<sub>2</sub>(dba)<sub>3</sub>, P(*o*-tol)<sub>3</sub>, chlorobenzene, reflux, 3 days.

We have developed a novel, highly planar and weakly electron-deficient moiety bis(2-ethylhexyl) 2,5-bis(5-bromothiophen-2-yl)thieno[3,2-b]thiophene-3,6-dicarboxylate (TT-Th) to construct a wide bandgap polymer donor PBDT-TT with BDT as the donor unit (Figure 3). Two weak electron withdrawing units, i.e. carboxylic ester, were introduced to the electron-rich backbone of TT and spurred it as a weak electron-deficient acceptor part. In addition, an unsubstituted thiophene was inserted between the BDT unit and the carboxylated substituted TT as bridge to reduce the steric hindrance.

As expected, PBDT-TT thin film shows an intense absorption spectrum in the region of 400~650 nm and appropriate HOMO (-5.23 eV) which can simultaneously match with ITIC-analogues and NIR acceptors. Consequently, when the ITIC-analogues as acceptor

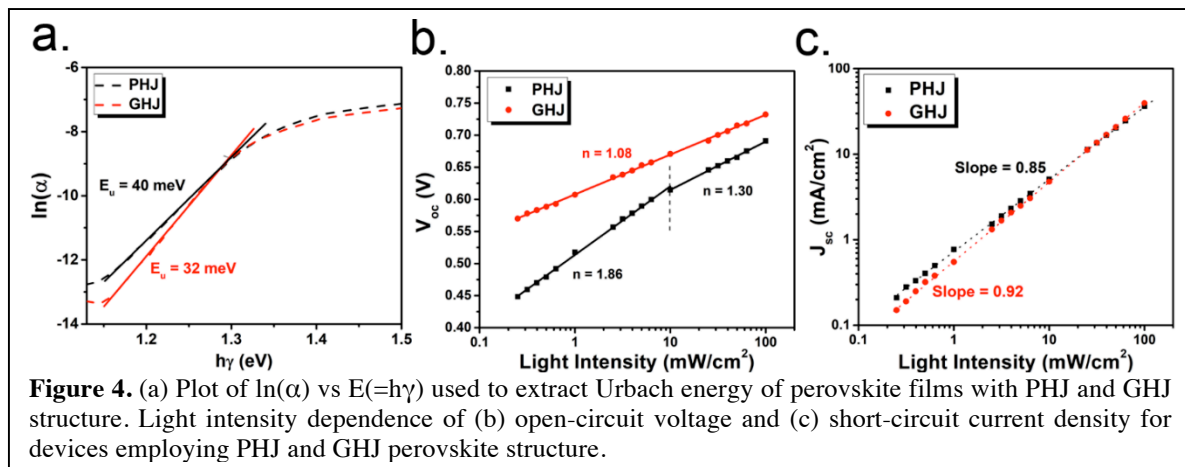
(absorption onset around 800 nm), the optimized PSCs devices based on the PBDT-TT:ITIC and PBDT-TT:IT-M (**Figure 3a**) exhibit a PCE of 9.67% and 11.38% with a high fill factor (FF) of 0.68 and 0.71, respectively. Meanwhile, the device based on PBDT-TT with a NIR acceptor 6TIC also show a high efficiency of 11.03% with a superior short circuit current ( $J_{sc}$ ) of  $21.4 \text{ mA/cm}^2$ , which owing to the broad absorption of NIR acceptor 6TIC extended to 950 nm. It is notable that the wide bandgap polymer PBDT-TT is one of the most efficient donor that can simultaneously match with ITIC-analogues and NIR acceptors in NF-PSCs with PCE over 11%. The results indicate that TT-Th is a promising new weak electron-deficient moiety for constructing efficient wide bandgap polymers and PBDT-TT is another promising candidate for high performance NF-PSCs.

### ***Defect passivation via graded fullerene heterojunction in low bandgap Pb-Sn binary perovskite solar cells***

Development of low bandgap ( $\sim 1.2 \text{ eV}$ ) Pb-Sn binary perovskites are exciting and have recently gained immense attention because of their high photovoltages, lowered Pb toxicity and its pivotal role in realizing perovskite tandem solar cell.<sup>[22-25]</sup> To further improve the optoelectronic quality and reduce photovoltage deficit for this class of low bandgap perovskites, it is important to reduce the density of trap sites, which adversely impacts the open-circuit voltage ( $V_{oc}$ ), charge collection efficiency and device performance.<sup>[26]</sup> Trap sites usually stem from facile point defect formation in the perovskite crystals and uncoordinated bonding at the film surface. Particularly for Sn-based perovskites, Sn cation vacancies have been identified as an additional critical factor that could deteriorate perovskite semiconductor properties.<sup>[27]</sup> Recent studies reporting perovskite-fullerene interactions/heterojunctions in Pb-based perovskites provide some insights for overcoming these issues due to defects. First, the trap sites in perovskite thin films could be passivated by applying fullerene derivatives, like C60 or PCBM.<sup>[28]</sup> As a result, the electronic properties of the derived device could be effectively enhanced and the hysteresis phenomena were significantly suppressed. Second, the fullerene derivatives could be applied as an efficient ETL for PVSCs since it has appropriate charge transport properties and lowers the resistance at perovskite/ETL interface.

In this program, we have studied the passivation of defect sites in low bandgap  $\text{CH}_3\text{NH}_3\text{Pb}_{0.5}\text{Sn}_{0.5}\text{I}_3$  perovskite through the incorporation of fluoroalkyl-substituted fullerene (DF-C60) via a graded heterojunction (GHJ) structure. Graded distribution of DF-C60 successfully reduced number of trap sites and the resultant films had characteristically lower Urbach energy, dominant bimolecular recombination, and higher surface / bulk recombination resistance.<sup>[29]</sup> The improved optoelectronic quality of films with GHJ structure reflected in improved performance for corresponding photovoltaic devices, with best PCE up to 15.61% and a remarkably high  $V_{oc}$  of 0.89 V. A  $V_{oc} \sim 92\%$  of the Shockley-Queisser (SQ) limit achieved here is comparable to that of state-of-the-art inorganic technologies and is the best among PVSCs till date. Additionally, through stability studies, we found that though GHJ with DF-C60 can slow down degradation due to moisture penetration, the oxidative susceptibility of Sn in binary perovskites sharply constraints overall stability.

To understand the improved optoelectronic quality of films with GHJ structure compared to PHJ structure, we characterized the absorption band edges. The band-edge of perovskite thin film with GHJ structure is sharper than the film with PHJ structure. Urbach energy ( $E_u$ ), which is the energetic disorder at the band edge, can be derived using the relation:  $\alpha = \alpha_0 \exp(E/E_u)$ , where  $\alpha$  is the absorption coefficient,  $E(=h\nu)$  is the photon energy, and  $E_u$  is the Urbach energy. As shown in **Figure 4**, the control PHJ sample has  $E_u \sim 40$  meV, whereas the GHJ sample has an  $E_u$  of  $\sim 32$  meV, which is  $\sim 20\%$  lower. This indicates that the incorporated DF-C60 with a gradient distribution lowers density of trap sites and sharpens band edge in Pb-Sn binary perovskites. Films with GHJ structure will thus have a lower trap-assisted recombination, which explains the improvement in  $V_{oc}$  for GHJ compared to PHJ.



To further elucidate the improved optoelectronic quality and understand charge recombination process in Pb/Sn-binary perovskites with different structures, light-intensity dependent current-voltage characterization measurement was performed. **Figure 4b-c** show the light-intensity-dependence of  $V_{oc}$  and  $J_{sc}$ , respectively. The  $V_{oc}$  is related to the splitting of the quasi-Fermi levels of electrons and holes with the quasi-Fermi level positions set by the free-carrier concentration, which in turn are determined by the balance between the photogeneration and recombination rates. The relationship between  $V_{oc}$  and light intensity ( $I$ ) is:  $V_{oc} = nkT/e \ln(I/I_0 + 1)$ , where  $n$  is the ideality factor,  $e$  is the elementary charge,  $k$  is the Boltzmann constant, and  $T$  is the temperature. For a trap-free, complete bimolecular recombination,  $n$  should be close to unity. On the other hand, if trap-assisted Shockley-Read-Hall (SRH) recombination dominated, the ideality factor  $n$  approaches 2. In the case of PHJ, the ideality  $n \sim 1.86$  at low incident light intensities ( $< 10$  mW/cm<sup>2</sup>) implying dominant SRH type recombination in this region. However, at the higher irradiance regime from 10 to 100 mW/cm<sup>2</sup>, the ideality  $n \sim 1.30$  approaches bimolecular limit. In the case of the GHJ devices, the  $n \sim 1.08$  was observed across the entire range of light intensity (from 2 to 100 mW/cm<sup>2</sup>). Further, according to the power law dependence between  $J_{sc}$  and  $I$ , the light intensity dependence of  $J_{sc}$  (**Figure 4c**) demonstrate that the GHJ PVSC has a higher slope of 0.92 compared to 0.85 for PHJ PVSCs, indicating the reduced extent of non-radiative trap assisted recombination with GHJ. These results definitively establish that bimolecular recombination is dominating in the GHJ devices and trap states in the GHJ perovskite thin films are far lesser than the PHJ thin films. The incorporated DF-C60 thus contribute towards passivation of defect states in perovskite thin-films which effectively enhances the perovskite optoelectronic quality and improves device performance.

➤ *Collaboration with Prof. Wen-Chang Chen at National Taiwan University (NTU)*

***Mechanically Robust, Stretchable Organic Solar Cells via Buckle-On-Elastomer Strategy***

We have actively collaborated with Prof. Chen's group at NTU during this period. In this report period, we focus on the development of stretchable organic solar cells (OSCs). In recent years, the exploitation of stretchable organic solar cell (OSC) has attracted significant research interests due to the rapid progress of wearable electronics. However, the development of a stretchable OSC is quite challenging since it has a strict requirement for the mechanical deformability and durability of each constituent layer in device. It shows the success exploitation of efficient stretchable OSCs necessitates the integration of material and device engineering. Herein, we first utilized the buckle-on-elastomer strategy to prepare mechanically robust, stretchable inverted OSCs with much improved efficiencies by using more advanced BHJ system. The completed flexible device stacks were first fabricated on a PEN substrate (2.5  $\mu\text{m}$  thick) and then were attached onto a pre-strained 3M elastomeric tape as illustrated in **Figure 5**.

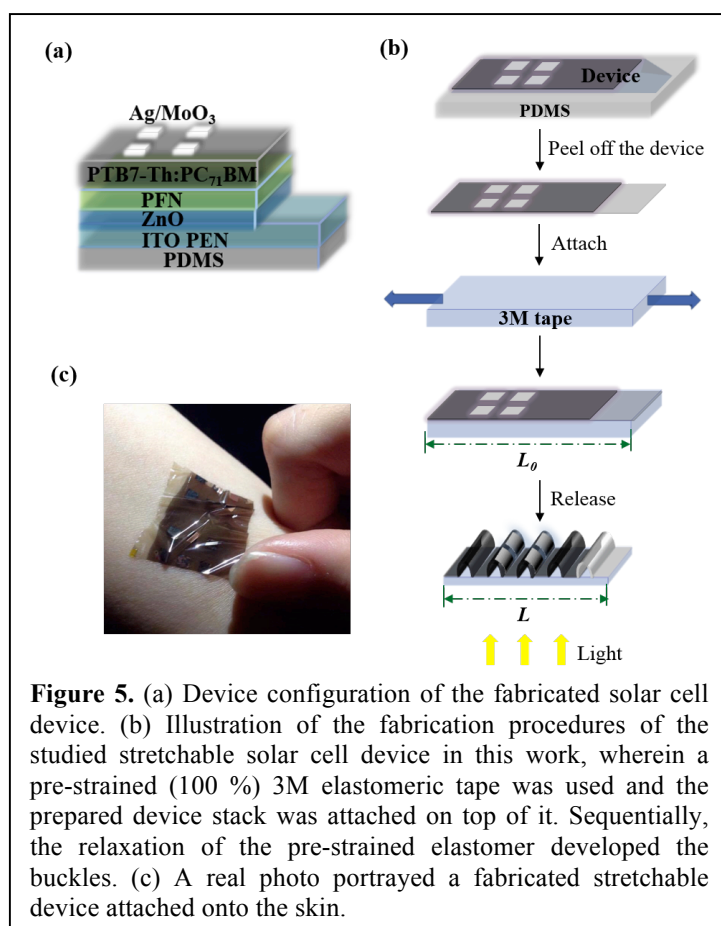


**Figure 5.** (a) Device configuration of the fabricated solar cell device. (b) Illustration of the fabrication procedures of the studied stretchable solar cell device in this work, wherein a pre-strained (100 %) 3M elastomeric tape was used and the prepared device stack was attached on top of it. Sequentially, the relaxation of the pre-strained elastomer developed the buckles. (c) A real photo portrayed a fabricated stretchable device attached onto the skin.

Owing to the pre-strained status of the elastomer, the ensemble wrinkle will be formed in response to accommodate the strain once the pre-strain was released, which can afford the derived OSC with a much improved mechanically robustness and stretchability. As shown, once the pre-strain force applied onto the elastomer is released, random buckling scaffold is formed in response to accommodate the strain (**Figure 6**).

We demonstrated that a pristine efficient (PCE: 5.61 %) OSC using such buckling scaffold can still preserve a high PCE of 4.13 % even under 30 % compression. The effects of mechanical deformation and durability on the electrical performance are investigated to reveal that such good mechanically robustness stems from the intact film morphology under

compression. More intriguingly, we demonstrated that such device can still retain its 64.3% efficiency after 50-cycle compression-stretching testing from 0 % to 30 % compression (**Figure 7**). This result disclosed that the stretchable inverted OSCs using random buckling architecture can have an outstanding compression-stretching endurance, revealing promising

potential for applications in large-scale and wearable OSC production.

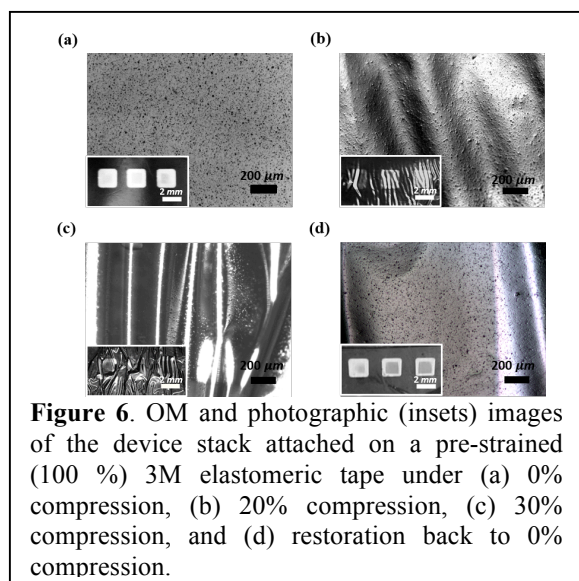


**Figure 6.** OM and photographic (insets) images of the device stack attached on a pre-stretched (100 %) 3M elastomeric tape under (a) 0% compression, (b) 20% compression, (c) 30% compression, and (d) restoration back to 0% compression.

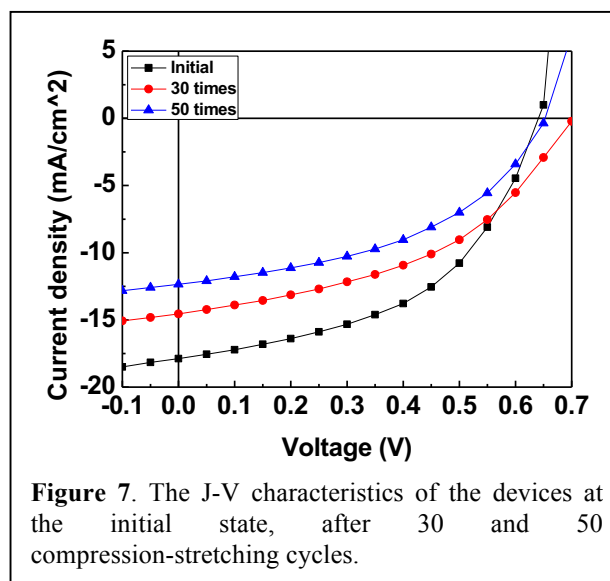


**Figure 7.** The J-V characteristics of the devices at the initial state, after 30 and 50 compression-stretching cycles.

### *Intrinsically Stretchable Nanostructured Silver Electrodes for Realizing Efficient Strain Sensors and Stretchable Organic Photovoltaic*

In addition to using the buckle-on-elastomer strategy, we also develop a durable and deformable transparent electrode fabricated without the pre-strain treatment and target to replace the ITO electrode. We first adopted polyethyleneimine (PEI) as the metal-chelating layer and then fabricated the hybrid electrodes on a 3M<sup>TM</sup> tape with a multilayer structure of SiO<sub>2</sub>/PEI/Ag(12nm)/modified PEDOT:PSS (**Figure 8**). The 3M<sup>TM</sup> tape herein was used as an efficient stretchable and adhesive substrate and the thin solution-processed SiO<sub>2</sub> layer was added to improve the light incoupling into the derived device. As for the inserted PEI layer, it can simultaneously improve the optoelectronic properties and stretchability of atop thin Ag film. Similarly, the Zonyl surfactant was added into PEDOT:PSS to enhance its mechanical stability.<sup>[30]</sup> Consequently, such hybrid electrode was revealed to have high electrical conductivity (>10<sup>5</sup> S cm<sup>-1</sup>), high elastic moduli (ca. 10<sup>2</sup> GPa), high transmittance (> 70%) across 400 to 900 nm, and decent stretchability (100% of the original conductivity can be retained after 50-cycle stretching under a 20% strain without pre-strain treatment), which is very suitable for serving as an efficient stretchable electrode.<sup>[31]</sup> We manifested the good stretchability of this hybrid

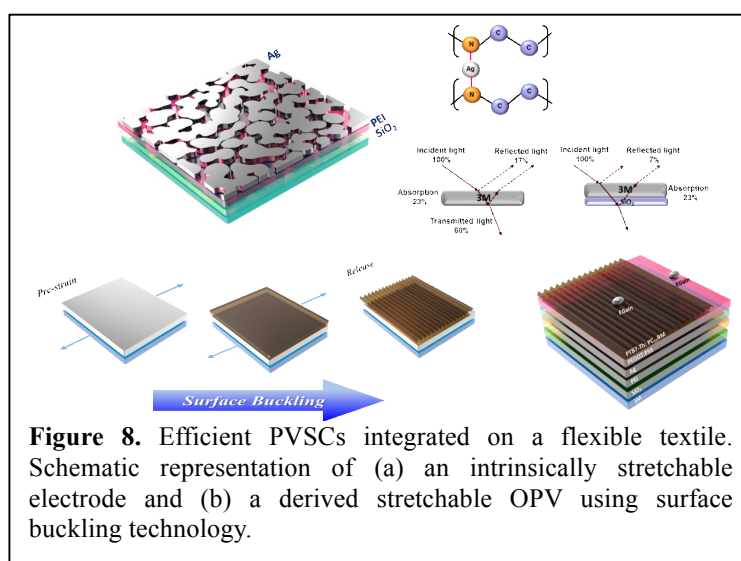
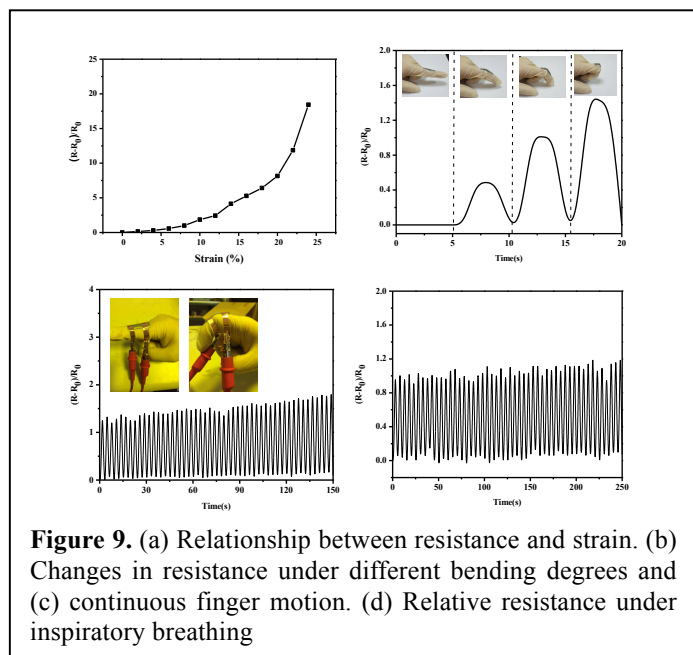


**Figure 8.** Efficient PVSCs integrated on a flexible textile. Schematic representation of (a) an intrinsically stretchable electrode and (b) a derived stretchable OPV using surface buckling technology.

As for the inserted PEI layer, it can simultaneously improve the optoelectronic properties and stretchability of atop thin Ag film. Similarly, the Zonyl surfactant was added into PEDOT:PSS to enhance its mechanical stability.<sup>[30]</sup> Consequently, such hybrid electrode was revealed to have high electrical conductivity (>10<sup>5</sup> S cm<sup>-1</sup>), high elastic moduli (ca. 10<sup>2</sup> GPa), high transmittance (> 70%) across 400 to 900 nm, and decent stretchability (100% of the original conductivity can be retained after 50-cycle stretching under a 20% strain without pre-strain treatment), which is very suitable for serving as an efficient stretchable electrode.<sup>[31]</sup> We manifested the good stretchability of this hybrid

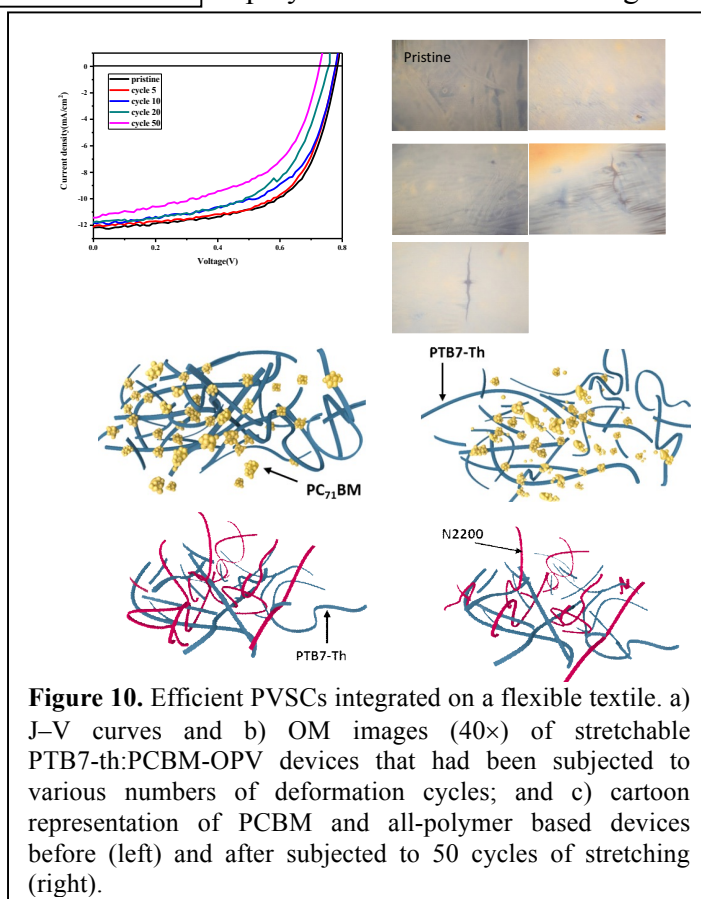
electrode resulted from the reversible phase separation endowed by the nano-cerebral morphology formed in Ag film.



When fabricating a resistive-type strain sensor using this hybrid electrode, a large gauge factor ( $GF \geq 30$ ) and stretchability ( $\geq 20\%$ ) can be obtained (**Figure 9**). This performance is rivaling with the results reported in the literatures.<sup>[32]</sup> Since the hybrid electrode is constructed on a 3M<sup>TM</sup> tape, the whole device stack could be readily attached onto a human body to receive such information as the respiratory rate and the motion of physiological behavior, revealing its great merit in personalized health-care systems. Moreover, representative fullerene-based and l-polymer based OPVs using this

electrode were fabricated and demonstrated superior stretchability. For the *PTB7-th*:PC<sub>71</sub>BM blend, the derived OPV can yield a decent PCEs of 6.0% along with high deformability (surface buckling treatment was employed to reinforce the mechanical properties of the *PTB7-th*:PC<sub>71</sub>BM active layer) under a 20% tensile strain, for which 75% of its initial PCE can be retained after 50 deformation cycles (**Figure 10**).

Meanwhile, the all-polymer OPV derived from the *PTB7-th*:N2200 blend can maintains over 96% of its original PCE after 50-cycles stretching (under a 20% strain) without using the wrinkled structure, benefitting from the better mechanical stretchability of N2200 over PC<sub>71</sub>BM.



**List of Publications and Significant Collaborations that resulted from AOARD supported project:**

**a) Papers published in peer-reviewed journals**

1. Z. B. Yang, C. C. Chueh, P. W. Liang, M. Crump, F. Lin, Z. L. Zhu, Alex K. Y. Jen, "Effects of Formamidinium and Bromide Ion Substitution in Methylammonium Lead Triiodide toward High-Performance Perovskite Solar Cells" *Nano Energy* **2016**, 22, 328-337.
2. Z. L. Zhu, C. C. Chueh, F. Lin, Alex K. Y. Jen, "Enhanced Ambient Stability of Efficient Perovskite Solar Cells by Employing a Modified Fullerene Cathode Interlayer", *Adv. Sci.*, **2016**, 3, 1600027.
3. Z. L. Zhu, Y. Bai, X. Liu, C. C. Chueh, S. H. Yang, Alex K. Y. Jen, "Enhanced Efficiency and Stability of Inverted Perovskite Solar Cells using Highly Crystalline SnO<sub>2</sub> Nanocrystals as the Robust Electron-Transporting Layer", *Adv. Mater.* **2016**, 28, 6478-6484.
4. D. B. Zhao, Z. L. Zhu, M. Y. Kuo, C. C. Chueh, Alex K. Y. Jen, "Hexaazatrinaphthylene Derivatives: A Class of Efficient Electron-Transporting Materials with Tunable Energy Levels for Inverted Perovskite Solar Cells", *Angew Chem .In. Ed.* **2016**, 55, 8999-9003.
5. Z. Yang, A. Rajagopal, C. C. Chueh, S. B. Jo, B. Liu, T. Zhao, Alex K. Y. Jen, "Stable Low Bandgap Pb-Sn Binary Perovskites for Tandem Solar Cells", *Adv. Mater.* **2016**, DOI: 10.1002/adma.201602696.
6. Z. L. Zhu, C. C. Chueh, G. Zhang, F. Huang, H. Yan, Alex K. Y. Jen, "Improved Ambient Stable Perovskite Solar Cells Enabled by a Hybrid Polymer Electron-Transporting Layer" *ChemSusChem* **2016**, 28, 8990-8997.
7. Z. Li, Z. L. Zhu, C. C. Chueh, S. B. Jo, J. D. Luo, S. H. Jiang, Alex K. Y. Jen, "Rational Design of Dipolar Chromophore with Intrinsic Radical Character as an Efficient Dopant-free Hole-Transporting Material for Perovskite Solar Cells", *J. Am. Chem. Soc.* **2016**, 138, 11833-11839.
8. X. Liu, C. C. Chueh, Z. L. Zhu, S. B. Jo, Y. Sun, Alex K. Y. Jen, "Highly Crystalline Zn<sub>2</sub>SnO<sub>4</sub> Nanoparticles as Efficient Electron-Transporting Layers toward Stable Inverted and Flexible Conventional Perovskite Solar Cells", *J. Mater. Chem. A* **2016**, 4, 15294-15301.
9. Z. L. Zhu, J. Q. Xu, C. C. Chueh, H. Liu, Z. Li, X. S. Li, H. S. Chen, Alex K. Y. Jen\*, "A Low-Temperature, Solution-Processable Organic Electron-Transporting Layer Based on Planar Coronene for High-performance Conventional Perovskite Solar Cells", *Adv. Mater.* **2016**, 28, 10786-10793.
10. X. L. F. Lin, C. C. Chueh, Q. Chen, T. Zhao, P. W. Liang, Z. L. Zhu, Y. Sun, Alex K. Y. Jen, "Fluoroalkyl-Substituted Fullerene/Perovskite Heterojunction for Efficient and Ambient Stable Perovskite Solar Cells", *Nano Energy* **2016**, 30, 417-425.
11. X. Liu, Z. Yang, C. C. Chueh, A. Rajagopal, S. T. Williams, Y. Sun, Alex K. Y. Jen, "Improved Efficiency and Stability of Pb-Sn Binary Perovskite Solar Cells by Cs Substitution", *J. Mater. Chem. A* **2016**, 4, 17939-17945.
12. Q. Wang, C. C. Chueh, M. Eslamian, Alex K. Y. Jen, "Modulation of PEDOT:PSS pH for Efficient Inverted Perovskite Solar Cells with Reduced Potential Loss and Enhanced Stability", *ACS Appl. Mater. Interfaces* **2016**, 8, 32068-32076.
13. Z. Yang, A. Rajagopal, S. B. Jo, C. C. Chueh, S. T. Williams, C. C. Huang, J. K.

- Katahara, H. W. Hillhouse, Alex K. Y. Jen, “Stabilized Wide Bandgap Perovskite Solar Cells by Tin Substitution”, *Nano Letter* **2016**, 16, 7739-7747.
14. N. Li, Z. L. Zhu, C. C. Chueh, H. B. Liu, B. Peng, A. Petrone, X. S. Li, L. D. Wang, Alex K. Y. Jen, “Mixed Cation  $\text{FA}_x\text{PEA}_{1-x}\text{PbI}_3$  with Enhanced Phase and Ambient Stability toward High-Performance Perovskite Solar Cells” *Adv. Energy Mater.* **2017**, 7, 1601307.
  15. C. C. Chueh, C. Z. Li, F. Z. Ding, Z. Li, N. Cernetic, X. S. Li, Alex K. Y. Jen\*, “Doping Versatile n-Type Organic Semiconductors via Room-Temperature Solution-Processable Anionic Dopants”, *ACS Appl. Mater. Interfaces.* **2017**, 9, 1136-1144.
  16. J. Y. Chen, C. C. Chueh, Z. L. Zhu, W. C. Chen, Alex K. Y. Jen, “Low-Temperature Electrodeposited Crystalline  $\text{SnO}_2$  as an Efficient Electron-Transporting Layer for Conventional Perovskite Solar Cells” *Sol. Energ. Mat. Sol. Cells* **2017**, 164, 47-55.
  17. X. B. Xu, C. C. Chueh, Z. B. Yang, A. Rajagopal, J. Q. Xu, S. B. Jo, Alex K. Y. Jen, “Ascorbic Acid as An Effective Antioxidant Additive to Enhance the Efficiency and Stability of Pb/Sn-Based Binary Perovskite Solar Cells”, *Nano Energy* **2017**, 34, 392-398.
  18. A. Rajagopal, P. W. Liang, C. C. Chueh, Z. Yang, Alex K. Y. Jen, “Defect Passivation via a Graded Fullerene Heterojunction in Low-Bandgap Pb-Sn Binary Perovskite Photovoltaics”, *ACS Energy Letters.* **2017**, 2, 2531-2539.
  19. Z. Zhu, D. Zhao, C. C. Chueh, X. Shi, Z. Li, Alex K. Y. Jen, “Highly Efficient and Stable Perovskite Solar Cells Enabled by All-Crosslinked Charge-Transporting Layers”, *Joule*, **2018**, 2, 168-183.
  20. Y. Y. Yu,\* C. H. Chen, C. C. Chueh, C. Y. Chiang, C. P. Chen\*, W. C. Chen\*, “Intrinsically Stretchable Nanostructured Silver Electrodes for Realizing Efficient Strain Sensors and Stretchable Organic Photovoltaics” *ACS Appl. Mater. Interfaces.* **2017**, 9, 27853-27862.
  21. J. Y. Lam, J. Y. Chen, P. C. Tsai, Y. T. Hsieh, C. C. Chueh\*, S. H. Tung\*, W. C. Chen\*, “A Stable, Efficient Textile-based Flexible Perovskite Solar Cell with Improved Washable and Deployable Capabilities for Wearable Device Applications” *RSC Adv.* **2017**, 7, 54361-54368.
  22. Y. T. Hsieh, J. Y. Chen, C. C. Shih, C. C. Chueh, W. C. Chen\*, “Mechanically Robust, Stretchable Organic Solar Cells via Buckle-On-Elastomer Strategy”, *Org. Electron.* **2018**, 53, 339-345.
  23. Y. T. Hsieh, J. Y. Chen, S. Fukuta, P. C. Lin, T. Higashihara, C. C. Chueh\*, W. C. Chen\*, “Realization of Intrinsically Stretchable Organic Solar Cells Enabled by Charge-Extraction Layer and Photoactive Material Engineering”, *ACS Appl. Mater. Interfaces.* **2018**, in press.
  24. X. Liao, Z. Yao, K. Gao, X. Shi, L. Zuo, Z. Zhu, L. Chen, F. Liu, Alex K. Y. Jen, “Mapping Non-Fullerene Acceptors with a Novel Wide Bandgap Polymers for High Performance Polymer Solar Cells”, *Adv. E. Mater.* **2018**, in press.

## b) Conference presentations

1. A. K.-Y. Jen, “Integrated Material, Interface, and Composition Engineering for High Performance Perovskite Solar Cells” 5th Sungkung International Solar Forum, Seoul, Korea, 25-May-2016.
2. A. K.-Y. Jen, “Material and Interface Engineering for High Performance Polymer and

- Perovskite Solar Cells”, Gordon Research Conference: Hybrid Electronic & Photonic Materials and Phenomena, Hong Kong, China, 21-Jun-2016.
3. A. K.-Y. Jen, “Material and Interface Engineering for High Performance Polymer and Perovskite Solar Cells”, International Conference on Synthetic Metals, Guangzhou, China, 28-Jun-2016.
  4. A. K.-Y. Jen, “Integrated Material, Interface, and Composition Engineering for High Performance Perovskite Solar Cells”, 4th International Workshop on Organic Composite Optoelectronic Materials and Devices, Qunshan, China, 24-Jul-16.
  5. A. K.-Y. Jen, “Tailored Interface for Improving Hysteresis and Stability of Perovskite Solar Cells”, ONR Workshop on Perovskite Solar Cell Stability, Seattle, USA, 11-Aug-2016.

## Reference

- [1] D. J. Lipomi, B. C. K. Tee, M. Vosgueritchian, Z. Bao, *Adv. Mater.* 2011, 23, 1771.
- [2] J. A. Rogers, T. Someya, Y. Huang, *Science* 2010, 327, 1603.
- [3] L. Hu, M. Pasta, F. L. Mantia, L. Cui, S. Jeong, H. D. Deshazer, J. W. Choi, S. M. Han, Y. Cui, *Nano Lett.* 2010, 10, 708.
- [4] X. Chen, H. Lin, P. Chen, G. Guan, J. Deng, H. Peng, *Adv. Mater.* 2014, 26, 4444.
- [5] L. Qiu, J. Deng, X. Lu, Z. Yang, H. Peng, *Angewandte Chemie-International Edition* 2014, 53, 10425.
- [6] H. Sun, X. You, Y. Jiang, G. Guan, X. Fang, J. Deng, P. Chen, Y. Luo, H. Peng, *Angewandte Chemie-International Edition* 2014, 53, 9526.
- [7] Z. Yang, J. Deng, H. Sun, J. Ren, S. Pan, H. Peng, *Adv. Mater.* 2014, 26, 7038.
- [8] H. Ma, H. L. Yip, F. Huang, A. K. Y. Jen, *Adv. Funct. Mater.* 2010, 20, 1371.
- [9] H.-L. Yip, A. K.-Y. Jen, *Energy Environ. Sci.* 2012, 5, 5994.
- [10] C. B. Nielsen, S. Holliday, H.-Y. Chen, S. J. Cryer, I. McCulloch, *Acc. Chem. Res.* 2015, 48, 2803.
- [11] Y. Lin, X. Zhan, *Adv. Energy Mater.* 2015, 5, 1501063.
- [12] Y. Lin, J. Wang, Z. G. Zhang, H. Bai, Y. F. Li, D. B. Zhu, X. W. Zhan, *Adv. Mater.* 2015, 27, 1170.
- [13] W. Zhao, D. Qian, S. Zhang, S. Li, O. Inganäs, F. Gao, J. Hou, *Adv. Mater.* 2016, 28, 4734.
- [14] W. Zhao, S. Li, H. Yao, S. Zhang, Y. Zhang, B. Yang, J. Hou, *J. Am. Chem. Soc.* 2017, 139, 7148.
- [15] Y. Cui, H. Yao, B. Gao, Y. Qin, S. Zhang, B. Yang, C. He, B. Xu, J. Hou, *J. Am. Chem. Soc.* 2017, 139, 7302.
- [16] Z. Fei, F.D. Eisner, X. Jiao, M. Azzouzi, J.A. Röhr, Y. Han, M. Shahid, A.S. Chesman, C.D. Easton, C.R. McNeill, T.D. Anthopoulos, J. Nelson, M. Heeney, *Adv. Mater.* 2018, 1705209.
- [17] X. Xu, T. Yu, Z. Bi, W. Ma, Y. Li, Q. Peng, *Adv. Mater.* 2017, 1703973.
- [18] H. Lin, S. Chen, Z. Li, J. Y. L. Lai, G. Yang, T. McAfee, K. Jiang, Y. Li, Y. Liu, H. Hu, J. Zhao, W. Ma, H. Ade, H. Yan, *Adv. Mater.* 2015, 27, 7299.
- [19] L. Gao, Z. Zhang, H. Bin, L. Xue, Y. Yang, C. Wang, F. Liu, T. P. Russell, Y. Li, *Adv. Mater.* 2016, 28, 8288.
- [20] H. Bin, Z. Zhang, L. Gao, S. Chen, L. Zhong, L. Xue, C. Yang, Y. Li, *J. Am. Chem. Soc.* 2016, 138, 4657.
- [21] H. Bin, L. Gao, Z. Zhang, Y. Yang, Y. Zhang, C. Zhang, S. Chen, L. Xue, C. Yang, M.

- Xiao, Y. Li, *Nature Commun.* 2016, 7, 13651.
- [22] L. A. Frolova, D. V. Anokhin, K. L. Gerasimov, N. N. Dremova, P. A. Troshin, *J. Phys. Chem. Lett.* 2016, 7, 4353.
- [23] M. T. Klug, A. Osherov, A. A. Haghighirad, S. D. Stranks, P. R. Brown, S. Bai, J. J. T.-W. Wang, X. Dang, V. Bulović, H. J. Snaith, et al., *Energy Environ. Sci.* 2017, 10, 236.
- [24] T. Krishnamoorthy, H. Ding, C. Yan, W. L. Leong, T. Baikie, Z. Zhang, M. Sherburne, S. Li, M. Asta, N. Mathews, et al., *J. Mater. Chem. A* 2015, 3, 23829.
- [25] S. T. Williams, A. Rajagopal, S. B. Jo, C.-C. Chueh, T. F. L. Tang, A. Kraeger, A. K.-Y. Jen, *J. Mater. Chem. A* 2017, 5, 10640.
- [26] J. M. Ball, A. Petrozza, *Nat. Energy* 2016, 1, 16149.
- [27] I. Chung, J.-H. Song, J. Im, J. Androulakis, C. D. Malliakas, H. Li, A. J. Freeman, J. T. Kenney, M. G. Kanatzidis, *J. Am. Chem. Soc.* 2012, 134, 8579.
- [28] J. Xu, A. Buin, A. H. Ip, W. Li, O. Voznyy, R. Comin, M. Yuan, S. Jeon, Z. Ning, J. J. McDowell, et al., *Nat. Commun.* 2015, 6, 7081.
- [29] X. Liu, F. Lin, C.-C. Chueh, Q. Chen, T. Zhao, P.-W. Liang, Z. Zhu, Y. Sun, A. K.-Y. Jen, *Nano Energy* 2016, 30, 417.
- [30] S. Savagatrup, E. Chan, S. M. Renteria-Garcia, A. D. Printz, A. V. Zaretski, T. F. O'Connor, D. Rodriquez, E. Valle, D. J. Lipomi, *Advanced Functional Materials* 2015, 25, 427.
- [31] D. McCoul, W. Hu, M. Gao, V. Mehta, Q. Pei, *Advanced Electronic Materials* 2016, 2, 1500407.
- [32] M. Amjadi, K.-U. Kyung, I. Park, M. Sitti, *Advanced Functional Materials* 2016, 26, 1678.